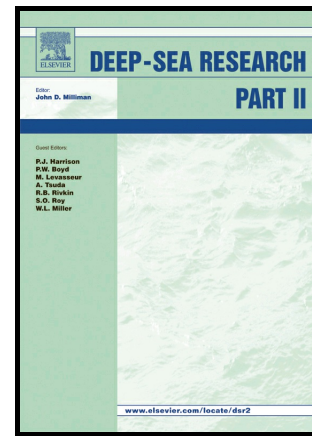


Author's Accepted Manuscript

Characteristics of the modelled meteoric freshwater budget of the western Antarctic Peninsula

J.M. van Wessem, M.P. Meredith, C.H. Reijmer,
M.R. van den Broeke, A.J. Cook



www.elsevier.com/locate/dsr2

PII: S0967-0645(16)30322-8

DOI: <http://dx.doi.org/10.1016/j.dsr2.2016.11.001>

Reference: DSR14150

To appear in: *Deep-Sea Research Part II*

Cite this article as: J.M. van Wessem, M.P. Meredith, C.H. Reijmer, M.R. van den Broeke and A.J. Cook, Characteristics of the modelled meteoric freshwater budget of the western Antarctic Peninsula, *Deep-Sea Research Part II* <http://dx.doi.org/10.1016/j.dsr2.2016.11.001>

This is a PDF file of an unedited manuscript that has been accepted for publication. As a service to our customers we are providing this early version of the manuscript. The manuscript will undergo copyediting, typesetting, and a review of the resulting galley proof before it is published in its final citable form. Please note that during the production process errors may be discovered which could affect the content, and all legal disclaimers that apply to the journal pertain.

1 Characteristics of the modelled meteoric freshwater 2 budget of the western Antarctic Peninsula

3 J. M. van Wessem^a, M. P. Meredith^b, C. H. Reijmer^a, M. R. van den Broeke^a,
4 A. J. Cook^c

5 ^a*Institute for Marine and Atmospheric Research Utrecht, Utrecht University, Utrecht, the*
6 *Netherlands*

7 ^b*British Antarctic Survey, Cambridge, United Kingdom*

8 ^c*Department of Geography, Durham University, Durham, United Kingdom*

9 **Abstract**

Rapid climatic changes in the western Antarctic Peninsula (WAP) have led to considerable changes in the meteoric freshwater input into the surrounding ocean, with implications for ocean circulation, the marine ecosystem and sea-level rise. In this study, we use the high-resolution Regional Atmospheric Climate Model RACMO2.3, coupled to a firm model, to assess the various contributions to the meteoric freshwater budget of the WAP for 1979–2014: precipitation (snowfall and rainfall), meltwater runoff to the ocean, and glacial discharge. Snowfall is the largest component in the atmospheric contribution to the freshwater budget, and exhibits large spatial and temporal variability. The highest snowfall rates are orographically forced and occur over the coastal regions of the WAP (>2000 mm water equivalent (w.e.) y^{-1}) and extend well onto the ocean up to the continental shelf break; a minimum (~ 500 mm w.e. y^{-1}) is reached over the open ocean. Rainfall is an order of magnitude smaller, and strongly depends on latitude and season, being large in summer, when sea ice extent is at its minimum. For Antarctic standards, WAP surface meltwater production is relatively large (>50 mm w.e. y^{-1}),

Email address: j.m.vanwessem@uu.nl (J. M. van Wessem)

Preprint submitted to Deep-Sea Research II, SI: WAP Marine Studies

November 3, 2016

but a large fraction refreezes in the snowpack, limiting runoff. Only at a few more northerly locations is the meltwater predicted to run off into the ocean. In summer, we find a strong relationship of the freshwater fluxes with the Southern Annular Mode (SAM) index. When SAM is positive and occurs simultaneously with a La Niña event there are anomalously strong westerly winds and enhanced snowfall rates over the WAP mountains, Marguerite Bay and the Bellingshausen Sea. When SAM coincides with an El Niño event, winds are more northerly, reducing snowfall and increasing rainfall over the ocean, and enhancing orographic snowfall over the WAP mountains. Assuming balance between snow accumulation (mass gain) and glacial discharge (mass loss), the largest glacial discharge is found for the regions around Adelaide Island (10 Gt y^{-1}), Anvers Island (8 Gt y^{-1}) and southern Palmer Land (12 Gt y^{-1}), while a minimum ($<2 \text{ Gt y}^{-1}$) is found in Marguerite Bay and the northern WAP. Glacial discharge is in the same order of magnitude as the direct freshwater input into the ocean from snowfall, but there are some local differences. The spatial patterns in the meteoric freshwater budget have consequences for local productivity and carbon drawdown in the coastal ocean.

10 *Keywords:* Western Antarctic Peninsula, Climate, Freshwater budget, Ocean,
11 Regional Climate Modelling

12 **1. Introduction**

13 During the second half of the twentieth century, the western Antarctic Penin-
14 sula (WAP) warmed more rapidly than any other region in the Southern Hemi-
15 sphere. Since 1950, the lower atmosphere above the WAP warmed by 3°C (King,
16 1994; Vaughan et al., 2003). This, in combination with increased ocean heat

17 content (Schmidtko et al., 2014), led to the loss of multiple ice shelves (Cook
18 and Vaughan, 2010), a retreat for 90% of its marine terminating glaciers (Cook
19 et al., 2014, 2016), an increase in precipitation (Thomas et al., 2008), and the
20 disappearance of most of the perennial sea ice (Stammerjohn et al., 2011). All
21 these changes affect the freshwater input (sea-ice melt and meteoric water, the
22 latter combining precipitation and glacial discharge) into the surrounding ocean,
23 significantly influencing the ecosystem, and, ultimately, the WAP contribution
24 to regional and global sea-level rise (Ivins et al., 2013; Rye et al., 2014). Ris-
25 ing atmospheric temperatures increase snow melt-rates and meltwater runoff into
26 the ocean (Vaughan, 2006). Intrusion of warm Circumpolar Deep Water (CDW)
27 originating from the Antarctic Circumpolar Current (ACC) onto and across the
28 continental shelf has been identified as the main cause of glacial ice loss in the
29 Amundsen Sea and likely in the Bellingshausen Sea (Martinson, 2012; Pritchard
30 et al., 2012), culminating in the retreat and calving of marine terminating glaciers
31 (Wouters et al., 2015; Cook et al., 2016). Together with the (partial) disintegra-
32 tion of WAP ice shelves, such as Wilkins Ice Shelf (Scambos et al., 2009), large
33 icebergs are formed that drift across the open ocean, releasing freshwater into the
34 ocean as they melt (Silva et al., 2006). Spatial and temporal changes in sea-ice
35 volume will significantly alter ocean temperature, salinity and stratification in the
36 vicinity of the WAP (Stammerjohn et al., 2008; Meredith et al., 2013). The ma-
37 rine ecology of the upper ocean adjacent to the WAP responds to these changes in
38 the freshwater budget (Meredith and King, 2005): freshening of the upper ocean
39 stabilizes the water column and enhances phytoplankton blooms (Montes-Hugo
40 et al., 2009); it also alters the ocean circulation by changing the geostrophic flow
41 (Martinson, 2012).

42 Measurements of stable isotopes of oxygen in seawater enable a quantitative
43 separation of the contributions of sea-ice melt and meteoric water to the total
44 freshwater budget (Meredith et al., 2008, 2010). Several studies used oxygen
45 isotope data from the Palmer Long-Term Ecological Research programme (Pal-
46 LTER; <http://pal.lternet.edu/>) and the Rothera Oceanographic and Biological Time
47 Series (RaTS; Clarke et al., 2008), as part of more comprehensive suites of physi-
48 cal, biogeochemical and biological measurements (Fig. 1). Some of these studies
49 have found that, as a result of the contributions of both glacial meltwater (Dierssen
50 et al., 2002) and precipitation (Meredith et al., 2008), the meteoric water flux is
51 the dominating freshwater source overall. However, a new study found that sea ice
52 melt contributions can be comparable to the meteoric water flux in specific years
53 because of the large interannual variability of the latter (Meredith et al., 2016).

54 It is thus clear that quantifying the spatial and temporal variability of the me-
55 teoric freshwater input is important for interpreting current and future changes
56 in the WAP. Meteoric freshwater fluxes depend on atmospheric forcing, includ-
57 ing the direction and magnitude of atmospheric water vapour transport (Meredith
58 et al., 2010). They are linked to subannual and interannual climate variability as
59 expressed in e.g. the Southern Annular Mode (SAM; Marshall, 2003; Thomas
60 et al., 2008), and the El Niño/Southern Oscillation phenomenon (ENSO, Wolter
61 and Timlin, 1993; Turner, 2004) and their interconnection (Clem and Fogt, 2013).
62 Moreover, model studies have found that precipitation rates over the WAP and the
63 adjacent ocean are extremely high due to strong orographic uplift (Van Wessem
64 et al., 2016). This affects both the direct (precipitation) and indirect (glacial dis-
65 charge) meteoric freshwater fluxes. Partitioning the contributions of these fluxes
66 is important as they affect the ecosystem in different ways: unlike precipitation,

67 glacial discharge can transport micronutrients and trace metals such as iron to the
68 ocean as the glaciers scour the underlying rock and sediment (Hawkings et al.,
69 2014). However, making this distinction from observations is difficult, especially
70 in the coastal areas where these fluxes are largest, as both water sources have a
71 similar isotopic composition and can be comparable in magnitude (Meredith et al.,
72 2013). An additional complication is the challenge of distinguishing basal melt-
73 ing from iceberg calving on the basis of ocean tracer data alone (Meredith et al.,
74 2013).

75 Atmospheric models provide information about meteoric freshwater input, but
76 are generally limited in horizontal resolution and hence do not resolve the large
77 spatial variability of WAP precipitation rates (Van Wessem et al., 2014a), are lim-
78 ited in simulation length (Van Lipzig et al., 2004; Bromwich, 2004), or have
79 limitations in their ability to resolve atmospheric and/or snow related processes
80 (Nicolas and Bromwich, 2011). In this study, we use the newest version of the Re-
81 gional Atmospheric Climate Model RACMO2.3 to address the above issues. The
82 model is run at high horizontal resolution (5.5 km) to properly simulate the large
83 spatial variability of the WAP topography and associated climate variables. The
84 model separately simulates the WAP meteoric freshwater components of snow-
85 fall, rainfall and meltwater for the period 1979–2014. The model is forced with
86 ERA-Interim, the most reliable re-analysis data for the Southern Ocean and tro-
87 posphere (Bracegirdle and Marshall, 2012), and is coupled to a Firn Densification
88 Model (FDM) that calculates processes in the snowpack such as the percolation
89 and refreezing of meltwater; runoff into the ocean is assumed to occur instanta-
90 neously at the snow/ice interface (Ettema et al., 2010; Ligtenberg et al., 2011).
91 Multiple studies evaluated the performance of RACMO2.3 by comparing model

92 output to observational data; the model has been proven to realistically simulate
93 the near-surface climate and surface mass balance of Antarctica (Van Wessem
94 et al., 2014a,b), as well as that of the Antarctic Peninsula (Van Wessem et al.,
95 2015, 2016). However, significant model biases remain: there is a cold surface
96 bias related to uncertainties in cloud cover and its relation to short- and longwave
97 radiation (Van Wessem et al., 2014a; King et al., 2015), and associated biases in
98 the melt-fluxes and the interaction of melt in the snowpack (Kuipers Munneke
99 et al., 2012; Barrand et al., 2013b). However, as we have shown in Van Wessem
100 et al. (2016), Antarctic Peninsula melt rates are small compared to the other fresh-
101 water fluxes, and these biases do not strongly influence the modelled freshwater
102 budget. First, in Section 2, we introduce the model and methods used. In Sections
103 3.1 and 3.2 we discuss the spatial and temporal variability of the meteoric fresh-
104 water components, and present an indirect estimate of WAP glacial discharge in
105 Section 3.3, based on long-term average surface mass balance fields and detailed
106 glacier catchment outlines. Finally, we discuss the results and present conclusions
107 in Section 4.

108 **2. Methods**

109 *2.1. RACMO2.3 and FDM*

110 We use the hydrostatic Regional Atmospheric Climate Model RACMO2.3.
111 Model settings are similar to Van Wessem et al. (2016). We only discuss model
112 output north of 70 °S, even though the simulations were conducted for a domain
113 extending as far south as 75 °S, in order to focus specifically on the WAP areas that
114 include the RaTS and Pal-LTER field sites. We included Larsen B ice shelf in the
115 model domain, even though it has collapsed during the period of the model run,

116 and will discuss the results accordingly. All further model details and a thorough
117 evaluation of model results are described in Van Wessem et al. (2014a, 2015,
118 2016).

119 RACMO2.3 is coupled to a FDM, a single column time-dependent model that
120 describes the evolution of the firn layer. It calculates firn density, temperature and
121 liquid water content evolution based on forcing at the surface by RACMO2.3 sur-
122 face temperature, accumulation and wind speed at 3 hourly resolution. The firn
123 layer has great spatial variability and has firn depths >100 m in high accumulation
124 regions. Surface meltwater percolates into the model firn layer, where it can re-
125 freeze, be stored or percolate further down. The retention of meltwater is based on
126 the 'tipping-bucket' method (i.e. liquid water is stored in the first available layer
127 and transported downwards only when it exceeds the maximum capillary reten-
128 tion). Liquid water that reaches the bottom of the firn layer is removed as runoff.
129 More details on the FDM can be found in Ligtenberg et al. (2011) and Kuipers
130 Munneke et al. (2015).

131 2.2. SAM and ENSO

132 To analyse temporal variations in the meteoric freshwater budget, we anal-
133 yse its sensitivity to the two leading modes of variability in the WAP region, i.e.
134 the Southern Annular Mode (SAM) and El Niño/Southern Oscillation (ENSO).
135 SAM is the leading mode of extratropical climate variability in the southern hemi-
136 sphere, defined as the meridional pressure difference between a node centered over
137 Antarctica and an annulus overlying the lower latitudes, and is associated with the
138 intensity of the westerly winds impinging on the WAP (Thompson, 2002). ENSO
139 variability originates in the tropical Pacific Ocean where it is most manifest, with
140 changes in sea surface temperature (SST) on timescales 4–7 years; this variability

141 reaches locations at high southern latitudes through both atmospheric and oceanic
142 teleconnections (Yuan, 2004; Turner, 2004). We have selected the upper/lower
143 quartiles (75%/25% percentiles) of monthly summer (December, January, Febru-
144 ary (DJF)) indices from the Marshall (2003) SAM index (SAM_{\pm}) and Wolter and
145 Timlin (1993) ENSO index ($ENSO_{\pm}$, where a positive index corresponds with
146 El Niño conditions) series. The percentile thresholds are chosen such that the
147 SAM/ $ENSO_{\pm}$ composites include ~ 10 months. We have specifically chosen to
148 analyse summer months, even though ENSO weakly correlates with summer con-
149 ditions in the AP (Clem and Fogt, 2013), given its importance for the freshwater
150 fluxes (see Sect. 3.2). We then extracted the average model output for the cor-
151 responding months, and, to account for possible interconnections between SAM
152 and ENSO, constructed $SAM_{\pm}/ENSO_{\pm}$ composite maps of the relevant freshwa-
153 ter components, and discuss temporal extremes in these variables by comparing
154 them with the 1979–2014 climatology.

155 2.3. *Glacier catchments and meteoric freshwater budget*

156 We calculated the average and integrated surface mass balance (SMB) for 676
157 glacier basins using delineations from Cook et al. (2014), to estimate glacial dis-
158 charge of the WAP. We assume that, as the majority of glaciers are retreating and
159 their retreat rates have recently accelerated (Pritchard et al., 2009; Cook et al.,
160 2014, 2016), the minimum glacial discharge equals the average long-term SMB;
161 the ice sheet is in steady state (ice discharge + SMB = 0). We furthermore as-
162 sume that the SMB averaged over the length of the model run (1979–2014) is
163 representative of the recent glacier history of the WAP. We separately calculate
164 the SMB for all basins that are larger than the size of one grid box ($\sim 30 \text{ km}^2$),
165 including all grid points that are within the basin outline for at least 50% of the

166 gridbox area. Because of the multitude of basins in this data-set, we binned the
167 data into 27 0.25° latitudinal intervals from 70° to 63.25°S , based on the average
168 latitude of the respective basin. In addition, to compare with glacial discharge, we
169 calculated the average freshwater input into the ocean by precipitation (snowfall
170 and rainfall). We integrated these fluxes over all WAP ocean grid-boxes up to the
171 continental shelf (Fig. 1) and binned them into the above latitudinal intervals.

172 **3. Results**

173 *3.1. Precipitation and snowmelt*

174 Figure 2 shows maps of the modelled average meteoric freshwater budget
175 components. These will only be briefly discussed here; a more detailed descrip-
176 tion of AP climate is provided in Van Wessem et al. (2016). Figure 2a shows large
177 snowfall rates over the western AP and the adjacent ocean, due to orographic up-
178 lift. Up to $2000\text{ mm w.e. y}^{-1}$ of snow falls over the ocean, de-
179 creasing steadily to the west, reaching $300\text{ mm w.e. y}^{-1}$ in the more distant ocean
180 around the continental shelf break. Over the western mountain range, snowfall
181 rates reach up to $5000\text{ mm w.e. y}^{-1}$, resulting in annual snow layers $>10\text{ m}$ deep.
182 In Marguerite Bay snowfall rates are variable, being surrounded by the mountain
183 ranges of Alexander Island, Adelaide Island and Palmer Land. The precipita-
184 tion shadow of Adelaide Island is most pronounced, with dry conditions (~ 200
185 mm w.e. y^{-1}) over Ryder Bay. Here, snowfall and rainfall (Fig. 2b) rates are sim-
186 ilar in magnitude; in most other locations rainfall is an order of magnitude smaller
187 than snowfall or zero. In sharp contrast with the spatial variability of snowfall,
188 which is mainly controlled by topography, gradients in rainfall are controlled by
189 latitude and elevation. Moreover, while snowfall occurs all year, rainfall is mostly

190 restricted to summer, when sea-ice extent is at its minimum. Therefore, summer
191 rainfall has a relatively large contribution to the freshwater flux into the ocean.
192 However, snowfall that accumulates on sea ice in winter, melts with the sea ice in
193 spring/summer, and at these locations the snowfall freshwater flux to the ocean is
194 delayed.

195 Surface snowmelt (Fig. 2c) is widespread over the WAP with sharp latitudinal
196 and elevation gradients. Meltwater has the potential to result in runoff into the
197 ocean when the firn layer has insufficient refreezing capacity (Kuipers Munneke
198 et al., 2014). Figure 2d shows that this rarely happens over the WAP; only in
199 lower-lying regions with low accumulation rates, and high meltwater production,
200 does some local meltwater runoff occur. Runoff is more frequent over Larsen B
201 and C ice shelves in the eastern AP (EAP) and on Wilkins ice shelf farther south.

202 Figure 3 shows modelled climatological and seasonal snowfall and rainfall
203 rates along four Pal-LTER transects. Along the four transects, average snowfall
204 rates over the ocean are roughly comparable (~ 500 mm w.e. y^{-1}), and all peak
205 towards the coast due to the orographic effect. Higher peak values are found for
206 the 300 and 600 transects, with a maximum >2000 mm w.e. y^{-1} for the 600 tran-
207 sect. While for transects 000, 300 and 600 snowfall rates rapidly decrease towards
208 the west, snowfall is low and constant in magnitude over the entire 900 transect.
209 This is related to the more northerly oriented slopes, which, in combination with
210 westerly winds, results in weaker orographic precipitation. Moreover, in contrast
211 to the other transects, the 900 transect shows an increase of rainfall towards the
212 northwest. Interannual variability (the red and blue shading) is closely related to
213 the absolute magnitude and does not show a relation with the location along the
214 transect, a feature that was also reported in Van Wessem et al. (2016).

215 It is important to note the seasonal precipitation cycle. Figure 3 shows that
216 summer snowfall, when the westerly circulation is weaker, is smaller than winter
217 snowfall by ~ 400 mm w.e. y^{-1} for all transects; this effect exceeds the interannual
218 variability of ~ 100 mm w.e. y^{-1} . As a result, the relative/fractional contribution
219 of rainfall is large in summer: for transects 900 and 600 rainfall reaches summer
220 values that are almost as large or even larger than that of snowfall, further empha-
221 sizing the importance of rainfall for the summertime meteoric freshwater budget
222 of the WAP.

223 No significant trends in any of the freshwater budget components for any of the
224 transects were found for the period 1979–2014, except for small negative trends in
225 rainfall near the coast that are related to cooling trends over the mountain slopes
226 as reported in Van Wessem et al. (2015).

227 3.2. SAM and ENSO climate variability

228 Temporal variability in the WAP freshwater budget has a strong relation to the
229 magnitude and the interconnection of both the circumpolar westerlies and forcing
230 from the tropics, which is reflected in variability associated with both SAM and
231 ENSO, respectively (Fogt et al., 2011; Clem and Fogt, 2013). We present com-
232 posite maps (SAM/ENSO \pm , see Section 2.2) of the meteoric freshwater fluxes
233 and compare them to the 1979–2014 climatology. We specifically provide maps
234 based on summer (DJF) months, even though snowfall rates are higher in winter
235 and ENSO shows a weak relation to summer conditions, because most snow falls
236 on the sea ice and melts in summer, and because of the relative importance of
237 summer compared to winter of the other fluxes (Section 3.1).

238 Figure 4 shows the freshwater flux anomalies, when the indices are in-phase
239 (SAM+ occurs during La Niña) and the ENSO connection to the AP region is

240 stronger than average (following Fogt et al. (2011); Clem and Fogt (2013)): when
241 SAM is high westerly circulation is anomalously strong and persistent over the
242 region, enhancing topographic precipitation in the WAP and reducing it in the
243 precipitation shadow of the AP spine. This is clearly shown in Figure 4a: during
244 SAM⁺ snowfall rates are highly elevated over the mountains (~ 100 mm w.e. y^{-1}),
245 slightly elevated over the adjacent ocean (~ 20 mm w.e. y^{-1}), and reduced by
246 ~ 20 mm w.e. y^{-1} in the EAP. In the WAP, even though snowfall is higher during
247 SAM⁺/ENSO⁻, rainfall is slightly lower, which is related to enhanced convection
248 and associated cooling, explaining the relatively low WAP warming compared to
249 the EAP during SAM⁺ (Marshall et al., 2006; van Lipzig et al., 2008). Snowmelt
250 dependency on SAM shows distinct patterns, with a negative anomaly to the west,
251 and a positive anomaly to the east, which is also consistent with earlier studies
252 (Marshall et al., 2006). This anomaly is a result of warm downslope winds, en-
253 hancing melt especially over the ice shelves. Consequently, runoff fluxes are high
254 over the EAP ice shelves during SAM⁺/ENSO⁻.

255 Figure 5 shows the freshwater flux anomalies, when the indices are out of
256 phase (SAM⁺ occurs during El Niño) and the ENSO connection to the AP region
257 is relatively weak (Clem and Fogt, 2013). Here, the westerly wind anomaly in-
258 cludes a stronger northerly component and the winds are more perpendicular to the
259 mountain range, enhancing the topographic snowfall further (>200 mm w.e. y^{-1}).
260 Moreover, the northwesterly winds advect warm air towards the WAP, enhanc-
261 ing rainfall and reducing snowfall over the Bellingshausen Sea. In addition, the
262 warmer air results in a positive snowmelt anomaly in the WAP, and enhances the
263 positive EAP snowmelt/runoff anomalies. An additional interesting feature is that
264 during SAM⁺/ENSO⁻ the wind anomaly blows into Marguerite Bay and Ryder

265 Bay, enhancing snowfall, while during SAM+/ENSO+ snowfall is reduced in Ry-
266 der Bay and parts of Marguerite Bay because it is in the precipitation shadow of
267 Adelaide Island, showing that this region is particularly sensitive to varying atmo-
268 spheric conditions. To further analyse the specific influence of ENSO, we have
269 looked at neutral and low values of the SAM indices, but found these results to be
270 inconclusive, likely due to the insignificant correlation of ENSO with the WAP in
271 summer (Clem and Fogt, 2013).

272 3.3. Glacial discharge and the meteoric freshwater budget

273 Figure 6 shows modelled climatological (1979–2014) specific surface mass
274 balance (SSMB) and the estimated meteoric freshwater budget: area integrated
275 SMB and runoff for WAP glacier basins, and ocean area integrated snowfall and
276 rainfall. Over the grounded WAP ice sheet, SSMB is defined as the area aver-
277 aged surface mass balance (SMB). Average and integrated SMB and runoff are
278 calculated for all WAP glacier basins defined by Cook et al. (2014). The fresh-
279 water fluxes are binned into 27 latitudinal intervals of 0.25° , ranging from 70°
280 to 63.25°S . Average and integrated snowfall and rainfall are computed over all
281 WAP ocean grid-boxes in the latitudinal bins up to the continental shelf. First, the
282 SSMB shows large latitudinal variability, with a clear maximum between 66.25°
283 and 65.75°S , where $\text{SSMB} > 5 \text{ m w.e. y}^{-1}$, coinciding with the region of largest
284 snowfall rates, just north of Adelaide Island (Fig. 2a). In this region WAP sur-
285 face elevation is the largest, resulting in efficient orographic precipitation. The
286 minimum SSMB is found in southern Palmer Land, with values $\sim 1 \text{ m w.e. y}^{-1}$.
287 The barplot in the left panel of Fig. 6 shows the SMB and meltwater runoff, inte-
288 grated over the glacier basins, and snowfall and rainfall, integrated over the ocean.
289 We assume that the average SMB over the length of the model run (36 years) is in

290 steady state with glacial discharge, providing a rough estimate of glacial discharge
291 along the WAP coast. Recent studies (Cook et al., 2014, 2016) found that ~90%
292 of WAP glaciers, and several northern AP glaciers (Scambos et al., 2014), are
293 retreating, especially to the south where retreat is strongest (Cook et al., 2014).
294 This implies that the average SMB likely provides a lower estimate of glacial
295 discharge. However, the timescale of AP glacial discharge can be longer than the
296 length of the model run (Barrand et al., 2013a). Therefore, real discharge rates can
297 also be lower than estimated for glacier basins with longer discharge timescales,
298 as large trends in WAP accumulation are found in decades prior to 1979 (Thomas
299 et al., 2008). The integrated snowfall and rainfall fluxes complete the meteoric
300 freshwater budget. We assume, as a first order estimate, that these fluxes, together
301 with glacial discharge, are redistributed in the adjacent WAP ocean. In reality the
302 AP coastal current (Moffat et al., 2008) will transport the freshwater components
303 southwards.

304 We find the highest basin-integrated SMB, and therefore the highest estimated
305 glacial discharge, in the 70°–69.5°S bins. Even though SSMB was lowest here,
306 this bin has by far the largest area (8000 km²), and ~12 Gt y⁻¹ of ice is dis-
307 charged into the ocean; at these high latitudes all surface meltwater refreezes,
308 and runoff is zero. Moving north, in the Marguerite Bay glacier basins (69°–
309 67.75°S), basin discharge ranges from 1.5 to 4 Gt y⁻¹; in the Adelaide Island bins
310 (67.25°– 66.75°S), area and glacial discharge peak are 4000 km² and 11 Gt y⁻¹,
311 respectively. Here, we also find the southernmost bin with significant modelled
312 runoff, but values are typically three orders of magnitude smaller than SMB, and
313 largely negligible. In the bins with the highest SSMB (bins 66.25° and 65.75°S),
314 the basins are relatively small (<2000 km²) and discharge is lower (<6 Gt y⁻¹).

315 The largest SMB for the northwestern AP is found between 65° and 64° S, the lo-
316 cation of Anvers Island, with values up to 8 Gt y^{-1} . Finally, in the northernmost
317 bins, discharge decreases to $\sim 2 \text{ Gt y}^{-1}$; a result of the small basin area and the
318 relatively low SSMB ($1\text{--}2 \text{ m w.e. y}^{-1}$).

319 In most bins the integrated snowfall fluxes have the same order of magnitude
320 as glacial discharge; evidently rainfall fluxes are small and increase in magnitude
321 towards the north, with the highest values up to 20% that of snowfall. There are
322 some locations where the snowfall fluxes show larger differences with discharge:
323 in the southern bins up to 67.5° S integrated snowfall fluxes are significantly larger
324 ($\sim 12 \text{ Gt y}^{-1}$) than discharge, except for the $69.75^{\circ}\text{--}69.5^{\circ}$ S bin, where the glacier
325 catchment area is the largest. This is due to both the small glacier basins and the
326 (nearly linear) increasing distance to the continental shelf and increasing ocean
327 area (no fluxes are computed for Alexander Island). Towards the north, the bins
328 near Adelaide Island stand out where discharge is twice as large as snowfall. Fi-
329 nally, in the two northernmost bins, where SSMB and SMB are both small, inte-
330 grated snowfall is larger than discharge.

331 **4. Summary and Conclusions**

332 The climate and associated freshwater budget of the western Antarctic Penin-
333 sula (WAP) is changing rapidly, with significant consequences for the surrounding
334 ocean, atmosphere and ecosystem. Here, we use the Regional Atmospheric Cli-
335 mate Model RAMCO2.3, for the period 1979–2014, to interpret temporal and spa-
336 tial variability in the meteoric freshwater budget: precipitation, meltwater runoff
337 and glacial discharge. We find that snowfall is the largest component in the at-
338 mospheric contribution to the meteoric freshwater budget. It shows large spatial

339 and seasonal variability, with average snowfall rates over the grounded ice sheet
340 >2000 mm w.e. y^{-1} due to orographic uplift of moist air over the steep AP moun-
341 tain range, decreasing to ~ 500 mm w.e. y^{-1} over the open ocean. Rainfall is an
342 order of magnitude smaller than snowfall, and is mainly determined by tempera-
343 ture, altitude and latitude. However, because rainfall is highest in summer, when
344 it is not intercepted by sea ice that is at its minimum, the contribution of rainfall to
345 the freshwater flux into the ocean is relatively large, and at lower latitudes nearly
346 as large as that of snowfall. The WAP meltwater production is large compared
347 to the rest of the Antarctic continent (>50 mm w.e. y^{-1}), but most meltwater re-
348 freezes in the cold snowpack; only at a few locations does meltwater run off into
349 the ocean, and this contribution to the freshwater budget is small.

350 Temporal variability of the freshwater components is related to the South-
351 ern Annular Mode (SAM) and El Niño/Southern Oscillation (ENSO) indices. In
352 summer, we find a strong relationship of the freshwater fluxes with SAM, and a
353 weak relation with ENSO. When high index states of SAM coincide with La Niña
354 events, snowfall is enhanced over Marguerite Bay and the Bellingshausen Sea.
355 Over the WAP orographic precipitation is enhanced and snowmelt reduced. When
356 SAM occurs during an El Niño event, winds are more northwesterly transporting
357 warmer air to the WAP, resulting in reduced snowfall and enhanced rainfall over
358 the ocean.

359 Finally, we use long-term average (1979–2014) modelled surface mass bal-
360 ance (SMB) to provide a rough estimate of glacial discharge. We find strong
361 latitudinal differences, with peak values in the regions around Adelaide Island
362 (10 Gt y^{-1}), Anvers Island (8 Gt y^{-1}) and southern Palmer Land (12 Gt y^{-1}).
363 Minima (<2 Gt y^{-1}) are found in Marguerite Bay and the northern WAP. As there

364 is a net mass loss of the majority of WAP glaciers, these estimates based on SMB
365 likely represent a lower limit for discharge. At most locations these fluxes are
366 in the same order of magnitude as the integrated snowfall fluxes into the ocean.
367 Integrated rainfall fluxes are an order of magnitude lower, peaking in the north.

368 The results of this study can, among other applications, be used to improve the
369 interpretation of seawater isotope datasets, as from such observations alone one
370 cannot readily distinguish between the different meteoric freshwater components,
371 often combining precipitation and glacial discharge fluxes as a single contribution.
372 A remaining challenge is a further partitioning of the glacial discharge flux into
373 the contributions made by basal melting and calving of icebergs.

374 **Acknowledgments**

375 This study is funded by the Netherlands Polar Program (NPP) and the Nether-
376 lands Organization of Scientific Research, section earth and Life Sciences section
377 (NWO/ALW).

378 **References**

379 Barrand, N. E., Hindmarsh, R. C. A., Arthern, R. J., Williams, C. R., Mougnot,
380 J., Scheuchl, B., Rignot, E., Ligtenberg, S. R. M., Van Den Broeke, M. R.,
381 Edwards, T. L., Cook, A. J., Simonsen, S. B., 2013a. Computing the volume
382 response of the Antarctic Peninsula ice sheet to warming scenarios to 2200.
383 *Journal of Glaciology* 59 (215), 397–409.

384 URL <http://www.igsoc.org/journal/59/215/t12J139.html>

385 Barrand, N. E., Vaughan, D. G., Steiner, N., Tedesco, M., Kuipers Munneke, P.,
386 Van den Broeke, M. R., Hosking, J. S., 2013b. Trends in Antarctic Peninsula

- 387 surface melting conditions from observations and regional climate modeling.
388 *Journal of Geophysical Research: Earth Surface* 118 (1), 315–330.
389 URL <http://doi.wiley.com/10.1029/2012JF002559>
- 390 Bracegirdle, T. J., Marshall, G. J., 2012. The reliability of antarctic tropospheric
391 pressure and temperature in the latest global reanalyses. *Journal of Climate* 25,
392 7138–7146.
- 393 Bromwich, D. H., 2004. Modeled Antarctic Precipitation. Part I: Spatial and Tem-
394 poral Variability. *Journal of Climate*, 427–448.
- 395 Clarke, A., Meredith, M. P., Wallace, M. I., Brandon, M. A., Thomas, D. N.,
396 sep 2008. Seasonal and interannual variability in temperature, chlorophyll and
397 macronutrients in northern Marguerite Bay, Antarctica. *Deep Sea Research*
398 Part II: Topical Studies in Oceanography 55 (18-19), 1988–2006.
399 URL <http://www.sciencedirect.com/science/article/pii/S0967064508001537>
- 400 Clem, K. R., Fogt, R. L., oct 2013. Varying roles of ENSO and SAM on the
401 Antarctic Peninsula climate in austral spring. *Journal of Geophysical Research:*
402 *Atmospheres* 118 (October), n/a–n/a.
403 URL <http://doi.wiley.com/10.1002/jgrd.50860>
- 404 Cook, A. J., Fox, A. J., Vaughan, D. G., Ferrigno, J. G., apr 2005. Retreating
405 glacier fronts on the Antarctic Peninsula over the past half-century. *Science*
406 (New York, N.Y.) 308 (5721), 541–4.
407 URL <http://www.ncbi.nlm.nih.gov/pubmed/15845851>
- 408 Cook, A. J., Holland, P. R., Meredith, M. P., Murray, T., Luckman, A., Vaughan,

409 D. G., 2016. Ocean forcing of glacier retreat in the western Antarctic Peninsula.
410 Science 353 (6296), 1261–1273.

411 Cook, A. J., Vaughan, D. G., feb 2010. Overview of areal changes of the ice
412 shelves on the Antarctic Peninsula over the past 50 years. The Cryosphere 4 (1),
413 77–98.

414 URL <http://www.the-cryosphere.net/4/77/2010/>

415 Cook, A. J., Vaughan, D. G., Luckman, A. J., Murray, T., nov 2014. A new
416 Antarctic Peninsula glacier basin inventory and observed area changes since
417 the 1940s. Antarctic Science 26 (06), 614–624.

418 URL http://www.journals.cambridge.org/abstract_S0954102014000200

419 Dierssen, H. M., Smith, R. C., Vernet, M., 2002. Glacial meltwater dynamics in
420 coastal waters west of the Antarctic peninsula. Proceedings of the National
421 Academy of Sciences of the United States of America 99 (4), 1790–1795.

422 URL <Go to ISI>://WOS:000174031100010\nhttp://www.ncbi.nlm.nih.gov/pmc/articles

423 Ettema, J., Van den Broeke, M. R., Van Meijgaard, E., Van de Berg, W. J., Box,
424 J. E., Steffen, K., dec 2010. Climate of the Greenland ice sheet using a high-
425 resolution climate model Part 1: Evaluation. The Cryosphere 4 (4), 511–527.

426 URL <http://www.the-cryosphere.net/4/511/2010/>

427 Fogt, R. L., Bromwich, D. H., Hines, K. M., apr 2011. Understanding the SAM
428 influence on the South Pacific ENSO teleconnection. Climate Dynamics 36 (7-
429 8), 1555–1576.

430 URL <http://link.springer.com/10.1007/s00382-010-0905-0>

- 431 Hawkings, J. R., Wadham, J. L., Tranter, M., Raiswell, R., Benning, L. G.,
432 Statham, P. J., Tedstone, A., Nienow, P., Lee, K., Telling, J., jan 2014. Ice
433 sheets as a significant source of highly reactive nanoparticulate iron to the
434 oceans. *Nature communications* 5, 3929.
435 URL <http://www.nature.com/ncomms/2014/140521/ncomms4929/full/ncomms4929.html>
- 436 Ivins, E. R., James, T. S., Wahr, J., O. Schrama, E. J., Landerer, F. W., Simon,
437 K. M., jun 2013. Antarctic contribution to sea level rise observed by GRACE
438 with improved GIA correction. *Journal of Geophysical Research: Solid Earth*
439 118 (6), 3126–3141.
440 URL <http://doi.wiley.com/10.1002/jgrb.50208>
- 441 King, J. C., 1994. Recent Climate Variability in the Vicinity of the Antarctic
442 Peninsula. *International Journal of Climatology* 14 (1987), 357–369.
- 443 King, J. C., Gadian, A., Kirchgassner, A., Kuipers Munneke, P., Orr, A., Reijmer,
444 C., Broeke, M. R., Van Wessem, J. M., Weeks, M., 2015. Validation of the sum-
445 mertime surface energy budget of Larsen C Ice Shelf (Antarctica) as represented
446 in three high-resolution atmospheric models. *Journal of Geophysical Research:*
447 *Atmospheres* 120 (4), 1335–1347.
- 448 Kuipers Munneke, P., Ligtenberg, S. R. M., Noël, B. P. Y., Howat, I. M., Box,
449 J. E., Mosley-Thompson, E., McConnell, J. R., Steffen, K., Harper, J. T., Das,
450 S. B., van den Broeke, M. R., jun 2015. Elevation change of the Greenland
451 ice sheet due to surface mass balance and firn processes, 1960–2013. *The*
452 *Cryosphere Discussions* 9 (3), 3541–3580.
453 URL <http://www.the-cryosphere-discuss.net/9/3541/2015/tcd-9-3541-2015.html>

454 Kuipers Munneke, P., Ligtenberg, S. R. M., Van Den Broeke, M. R., Vaughan,
455 D. G., 2014. Firn air depletion as a precursor of Antarctic ice-shelf collapse.
456 *Journal of Glaciology* 60 (220), 205–214.

457 URL <http://www.igsoc.org/journal/60/220/t13J183.html>

458 Kuipers Munneke, P., Picard, G., van den Broeke, M. R., Lenaerts, J. T. M., van
459 Meijgaard, E., jan 2012. Insignificant change in Antarctic snowmelt volume
460 since 1979. *Geophysical Research Letters* 39 (1), 6–10.

461 URL <http://www.agu.org/pubs/crossref/2012/2011GL050207.shtml>

462 Ligtenberg, S. R. M., Helsen, M. M., van den Broeke, M. R., oct 2011. An
463 improved semi-empirical model for the densification of Antarctic firn. *The*
464 *Cryosphere* 5 (4), 809–819.

465 URL <http://www.the-cryosphere.net/5/809/2011/>

466 Marshall, G., Orr, A., Van Lipzig, N., King, J., 2006. The Impact of a Changing
467 Southern Hemisphere Annular Mode on Antarctic Peninsula Summer Temper-
468 atures. *Journal of Climate* 19 (2001), 5388–5404.

469 Marshall, G. J., dec 2003. Trends in the Southern Annular Mode from Observa-
470 tions and Reanalyses. *Journal of Climate* 16 (24), 4134–4143.

471 URL [http://journals.ametsoc.org/doi/full/10.1175/1520-0442\(2003\)016%3C4134%3ATT](http://journals.ametsoc.org/doi/full/10.1175/1520-0442(2003)016%3C4134%3ATT)

472 Martinson, D. G., jun 2012. Antarctic circumpolar current's role in the Antarctic
473 ice system: An overview. *Palaeogeography, Palaeoclimatology, Palaeoecology*
474 335-336, 71–74.

475 URL <http://www.sciencedirect.com/science/article/pii/S0031018211001799>

- 476 Meredith, M. P., King, J. C., 2005. Rapid climate change in the ocean west of
477 the Antarctic Peninsula during the second half of the 20th century. *Geophysical*
478 *Research Letters* 32 (19), L19604.
479 URL <http://doi.wiley.com/10.1029/2005GL024042>
- 480 Meredith, M. P., Murphy, E. J., Hawker, E. J., King, J. C., Wallace, M. I., 2008.
481 On the interannual variability of ocean temperatures around South Georgia,
482 Southern Ocean: Forcing by El Niño/Southern Oscillation and the Southern
483 Annular Mode. *Deep-Sea Research Part II: Topical Studies in Oceanography*
484 55 (18-19), 2007–2022.
- 485 Meredith, M. P., Stammerjohn, S. E., Venables, H. J., Ducklow, H. W., Martinson,
486 D. G., Iannuzzi, R. A., Leng, M. J., Van Wesseem, J. M., Reijmer, C. H., Barrand,
487 N. E., 2016. Deep-Sea Research II Changing distributions of sea ice melt and
488 meteoric water west of the Antarctic Peninsula. *Deep-Sea Research Part II*, 1–
489 18.
490 URL <http://dx.doi.org/10.1016/j.dsr2.2016.04.019>
- 491 Meredith, M. P., Venables, H. J., Clarke, A., Ducklow, H. W., Erickson, M., Leng,
492 M. J., Lenaerts, J. T. M., van den Broeke, M. R., mar 2013. The Freshwater
493 System West of the Antarctic Peninsula: Spatial and Temporal Changes.
494 *Journal of Climate* 26 (5), 1669–1684.
495 URL <http://journals.ametsoc.org/doi/abs/10.1175/JCLI-D-12-00246.1>
- 496 Meredith, M. P., Wallace, M. I., Stammerjohn, S. E., Renfrew, I. A., Clarke,
497 A., Venables, H. J., Shoosmith, D. R., Souster, T., Leng, M. J., oct 2010.
498 Changes in the freshwater composition of the upper ocean west of the Antarctic
499 Peninsula during the first decade of the 21st century. *Progress in Oceanography*

500 87 (1-4), 127–143.

501 URL <http://www.sciencedirect.com/science/article/pii/S007966111000131X>

502 Moffat, C., Beardsley, R. C., Owens, B., van Lipzig, N., 2008. A first description
503 of the Antarctic Peninsula Coastal Current. *Deep Sea Research Part II: Topical
504 Studies in Oceanography* 55 (3), 277–293.

505 Montes-Hugo, M., Doney, S. C., Ducklow, H. W., Fraser, W., Martinson, D.,
506 Stammerjohn, S. E., Schofield, O., 2009. Recent Changes in Phytoplankton
507 Communities Associated with Rapid Regional Climate Change Along the West-
508 ern Antarctic Peninsula. *Science* 323 (March), 1470–1473.

509 Nicolas, J. P., Bromwich, D. H., mar 2011. Precipitation Changes in High South-
510 ern Latitudes from Global Reanalyses: A Cautionary Tale. *Surveys in Geo-
511 physics* 32 (4-5), 475–494.

512 URL <http://link.springer.com/10.1007/s10712-011-9114-6>

513 Pritchard, H. D., Arthern, R. J., Vaughan, D. G., Edwards, L. A., oct 2009. Exten-
514 sive dynamic thinning on the margins of the Greenland and Antarctic ice sheets.
515 *Nature* 461 (7266), 971–5.

516 URL <http://dx.doi.org/10.1038/nature08471>

517 Pritchard, H. D., Ligtenberg, S. R. M., Fricker, H. A., Vaughan, D. G., Van den
518 Broeke, M. R., Padman, L., apr 2012. Antarctic ice-sheet loss driven by basal
519 melting of ice shelves. *Nature* 484 (7395), 502–5.

520 URL <http://www.ncbi.nlm.nih.gov/pubmed/22538614>

521 Rye, C. D., Naveira Garabato, A. C., Holland, P. R., Meredith, M. P., George
522 Nurser, A. J., Hughes, C. W., Coward, A. C., Webb, D. J., aug 2014. Rapid sea-

- 523 level rise along the Antarctic margins in response to increased glacial discharge.
524 Nature Geoscience 7 (10), 732–735.
525 URL <http://dx.doi.org/10.1038/ngeo2230>
- 526 Scambos, T., Fricker, H. A., Liu, C.-C., Bohlander, J., Fastook, J., Sargent, A.,
527 Massom, R., Wu, A.-M., apr 2009. Ice shelf disintegration by plate bending and
528 hydro-fracture: Satellite observations and model results of the 2008 Wilkins
529 ice shelf break-ups. Earth and Planetary Science Letters 280 (1-4), 51–60.
530 URL <http://linkinghub.elsevier.com/retrieve/pii/S0012821X08007887>
- 531 Scambos, T. A., Berthier, E., Haran, T., Shuman, C. A., Cook, A. J., Ligtenberg, S.
532 R. M., Bohlander, J., nov 2014. Detailed ice loss pattern in the northern Antarc-
533 tic Peninsula: widespread decline driven by ice front retreats. The Cryosphere
534 8 (6), 2135–2145.
535 URL <http://www.the-cryosphere.net/8/2135/2014/>
- 536 Schmidtko, S., Heywood, K. J., Thompson, A. F., Aoki, S., dec 2014. Multi-
537 decadal warming of Antarctic waters. Science (New York, N.Y.) 346 (6214),
538 1227–31.
539 URL <http://www.sciencemag.org/content/346/6214/1227.short>
- 540 Silva, T. A. M., Bigg, G. R., Nicholls, K. W., 2006. Contribution of giant ice-
541 bergs to the Southern Ocean freshwater flux. Journal of Geophysical Research
542 111 (C3), C03004.
543 URL <http://doi.wiley.com/10.1029/2004JC002843>
- 544 Stammerjohn, S., Maksym, T., Heil, P., Massom, R. A., Vancoppenolle, M.,
545 Leonard, K. C., may 2011. The influence of winds, sea-surface temperature and

- 546 precipitation anomalies on Antarctic regional sea-ice conditions during IPY
547 2007. *Deep Sea Research Part II: Topical Studies in Oceanography* 58 (9-10),
548 999–1018.
549 URL <http://www.sciencedirect.com/science/article/pii/S0967064510003048>
- 550 Stammerjohn, S. E., Martinson, D. G., Smith, R. C., Iannuzzi, R. A., sep 2008.
551 Sea ice in the western Antarctic Peninsula region: Spatio-temporal variability
552 from ecological and climate change perspectives. *Deep Sea Research Part II:*
553 *Topical Studies in Oceanography* 55 (18-19), 2041–2058.
554 URL <http://www.sciencedirect.com/science/article/pii/S0967064508001562>
- 555 Thomas, E. R., Marshall, G. J., McConnell, J. R., jan 2008. A doubling in snow
556 accumulation in the western Antarctic Peninsula since 1850. *Geophysical Re-*
557 *search Letters* 35 (1), 1–5.
558 URL <http://www.agu.org/pubs/crossref/2008/2007GL032529.shtml>
- 559 Thompson, D. W. J., may 2002. Interpretation of Recent Southern Hemisphere
560 Climate Change. *Science* 296 (5569), 895–899.
561 URL <http://www.sciencemag.org/content/296/5569/895.short>
- 562 Turner, J., jan 2004. The El Niñosouthern oscillation and Antarctica. *International*
563 *Journal of Climatology* 24 (1), 1–31.
564 URL <http://doi.wiley.com/10.1002/joc.965>
- 565 Van Lipzig, N. P. M., King, J. C., Lachlan-Cope, T. A., 2004. Precipitation, subli-
566 mation, and snow drift in the Antarctic Peninsula region from a regional atmo-
567 spheric model. *Journal of Geophysical Research* 109 (D24), 1–16.
568 URL <http://www.agu.org/pubs/crossref/2004/2004JD004701.shtml>

- 569 van Lipzig, N. P. M., Marshall, G. J., Orr, A., King, J. C., apr 2008. The Relation-
570 ship between the Southern Hemisphere Annular Mode and Antarctic Peninsula
571 Summer Temperatures: Analysis of a High-Resolution Model Climatology.
572 *Journal of Climate* 21 (8), 1649–1668.
573 URL <http://journals.ametsoc.org/doi/abs/10.1175/2007JCLI1695.1>
- 574 Van Wessem, J. M., Ligtenberg, S. R. M., Reijmer, C. H., Van de Berg, W. J., Van
575 den Broeke, M. R., Barrand, N. E., Thomas, E. R., Turner, J., Wuite, J., Scam-
576 bos, T. A., Van Meijgaard, E., feb 2016. The modelled surface mass balance of
577 the Antarctic Peninsula at 5.5 km horizontal resolution. *The Cryosphere* 10 (1),
578 271–285.
579 URL <http://www.the-cryosphere.net/10/271/2016/>
- 580 Van Wessem, J. M., Reijmer, C. H., Lenaerts, J. T. M., Van de Berg, W. J., Van
581 den Broeke, M. R., Van Meijgaard, E., jan 2014a. Updated cloud physics in
582 a regional atmospheric climate model improves the modelled surface energy
583 balance of Antarctica. *The Cryosphere* 8 (1), 125–135.
584 URL <http://www.the-cryosphere.net/8/125/2014/>
- 585 Van Wessem, J. M., Reijmer, C. H., Morlighem, M., Mougnot, J., Rignot, E.,
586 Medley, B., Joughin, I., Wouters, B., Depoorter, M. A., Bamber, J. L., Lenaerts,
587 J. T. M., Van De Berg, W. J., Van Den Broeke, M. R., Van Meijgaard, E., 2014b.
588 Improved representation of East Antarctic surface mass balance in a regional
589 atmospheric climate model. *Journal of Glaciology* 60 (224), 761–770.
590 URL <http://www.igsoc.org/journal/60/222/t14j051.html>
- 591 Van Wessem, J. M., Reijmer, C. H., Van de Berg, W. J., Van den Broeke, M. R.,
592 Cook, A. J., Van Ulf, L. H., Van Meijgaard, E., 2015. Temperature and

- 593 Wind Climate of the Antarctic Peninsula as Simulated by a High-Resolution
594 Regional Atmospheric Climate Model. *Journal of Climate* 28 (18), 7306–7326.
595 URL <http://journals.ametsoc.org/doi/abs/10.1175/JCLI-D-15-0060.1>
- 596 Vaughan, D. G., 2006. Recent Trends in Melting Conditions on the Antarctic
597 Peninsula and Their Implications for Ice-sheet Mass Balance and Sea Level.
598 *Arctic, Antarctic, and Alpine Research* 38 (1), 147–152.
- 599 Vaughan, D. G., Marshall, G., Connolley, W. M., Parkinson, C., Mulvaney, R.,
600 Hodgson, D. A., King, J. C., Pudsey, C. J., Turner, J., 2003. Recent Rapid
601 Regional Climate Warming on the Antarctic Peninsula. *Climatic Change* 60,
602 243–274.
- 603 Wolter, K., Timlin, M., 1993. Monitoring ENSO in COADS with a seasonally
604 adjusted principal component index. *Proc. of the 17th Climate Diagnostics*.
605 URL <http://140.172.38.100/psd/enso/mei.ext/WT1.pdf>
- 606 Wouters, B., Martin-Español, A., Helm, V., Flament, T., van Wessem, J. M.,
607 Ligtenberg, S. R. M., van den Broeke, M. R., Bamber, J. L., may 2015. Dy-
608 namic thinning of glaciers on the Southern Antarctic Peninsula. *Science* (New
609 York, N.Y.) 348 (6237), 899–903.
610 URL <http://www.sciencemag.org/content/348/6237/899.abstract>
- 611 Yuan, X., dec 2004. ENSO-related impacts on Antarctic sea ice: a synthesis of
612 phenomenon and mechanisms. *Antarctic Science* 16 (4), 415–425.
613 URL http://journals.cambridge.org/abstract_S0954102004002238

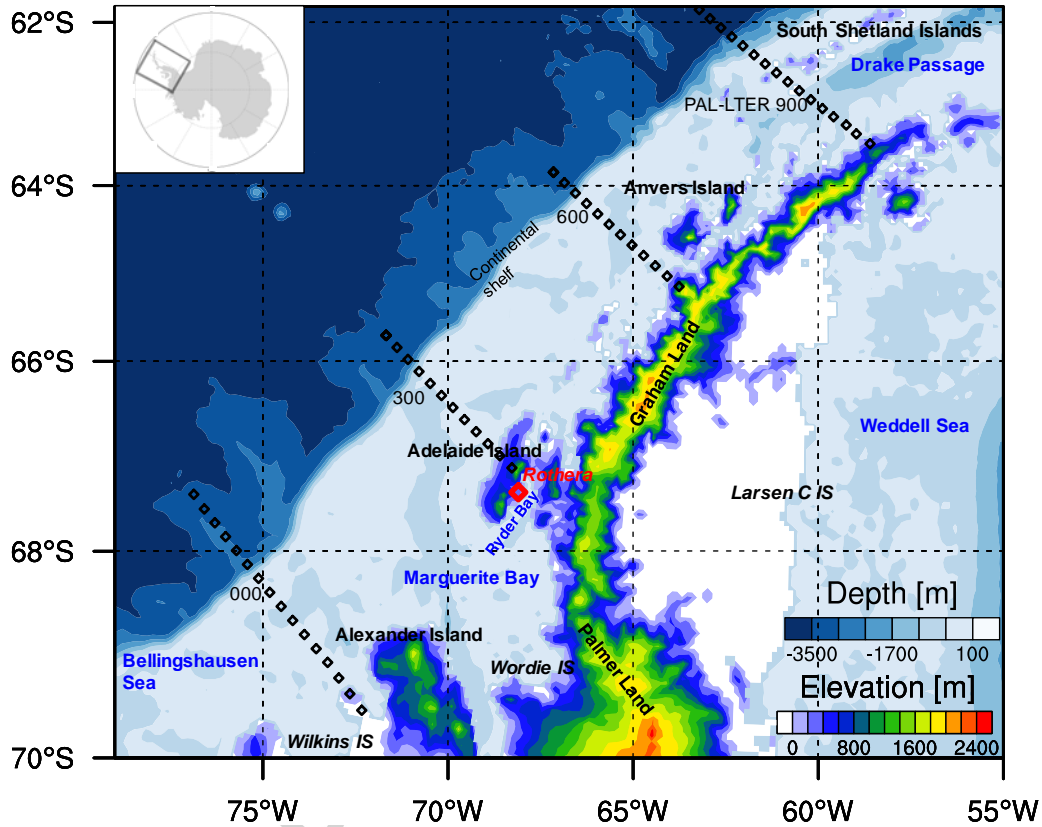


Figure 1: The northern ($>70^\circ$ S) Antarctic Peninsula (AP) domain (black box in inset map of Antarctica) shows the full AP RACMO2.3 model domain and boundaries, which extends to 75° S) with model surface topography [m] and ocean depth [m] of the AP. White areas represent floating ice shelves and regions over land with elevations <40 m, colours represent the elevation of the grounded ice sheet and ocean depth. Locations of four transects are shown (black diamonds), coinciding with survey lines from the Pal-LTER program, as used in Section 3.1. Some locations as used throughout the text are marked.

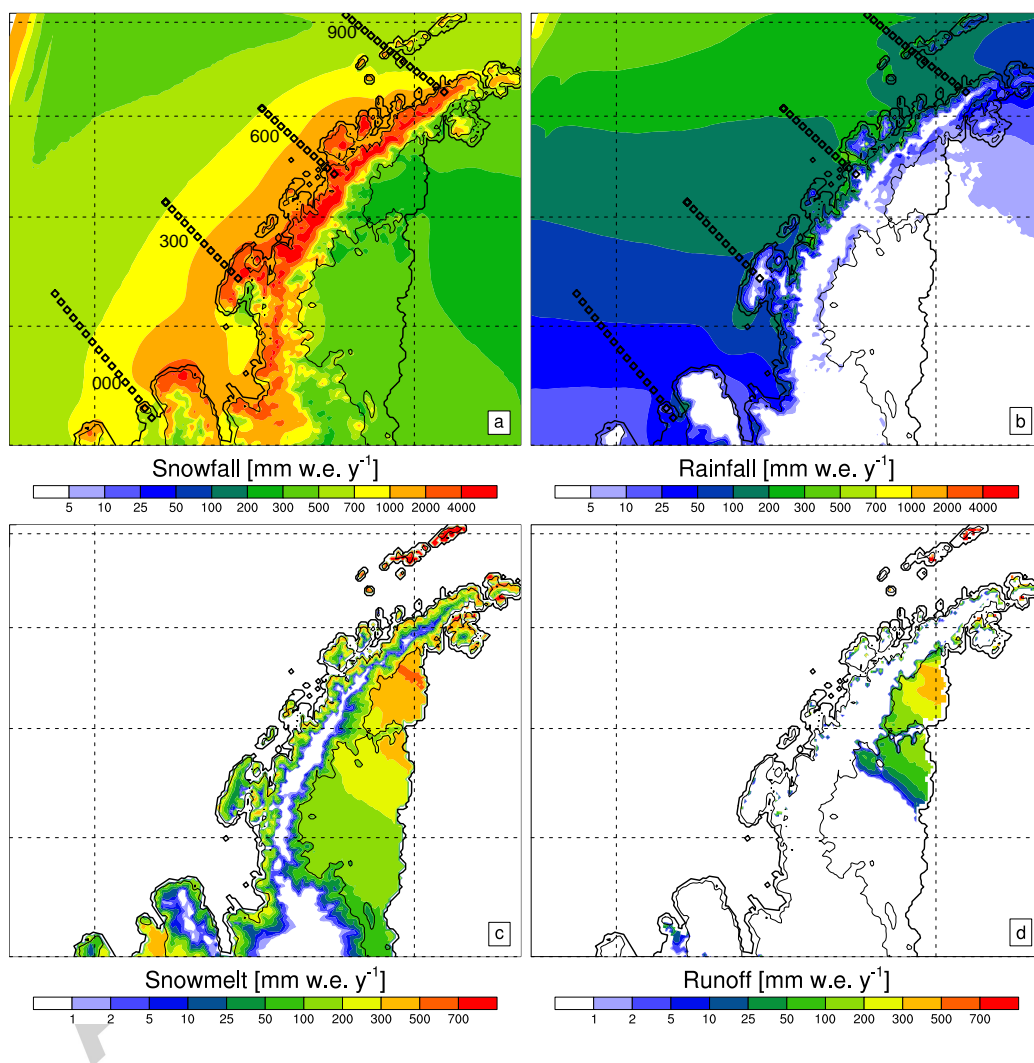


Figure 2: Climatological (1979–2014) freshwater fluxes from RACMO2.3: snowfall (a), rainfall (b), snowmelt (c) and meltwater runoff (d) in mm w.e. y⁻¹. Note the different scales in a,b compared to c,d. Also shown in a,b are the Pal-LTER transects as used in this study.

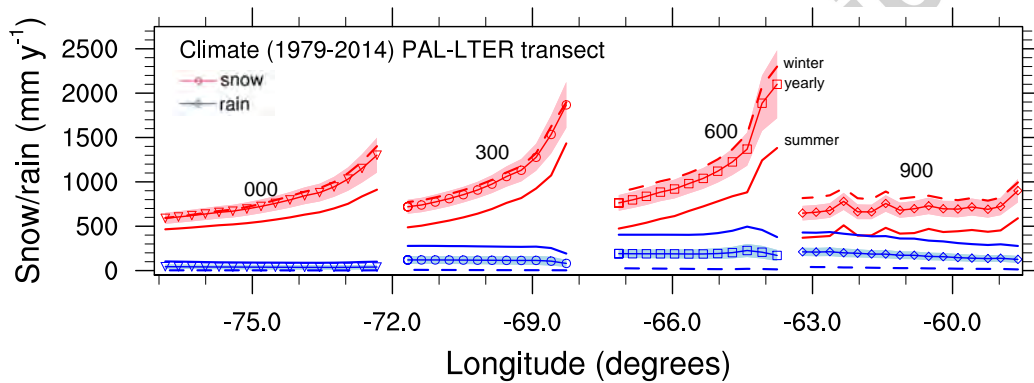


Figure 3: Climatological (1979–2014) snowfall (red) and rainfall (blue) (mm w.e. y^{-1}) across Pal-LTER transects (see Figs. 1 and 2) 900 (diamonds), 600 (squares), 300 (circles) and 000 (triangles). Shading denotes interannual variability (one standard deviation). The dashed lines denote the winter (Jun., Jul., Aug.) averages, the solid (unmarked) lines the summer (Dec., Jan., Feb.) averages. Each of the transects is extrapolated so as to include two land points.

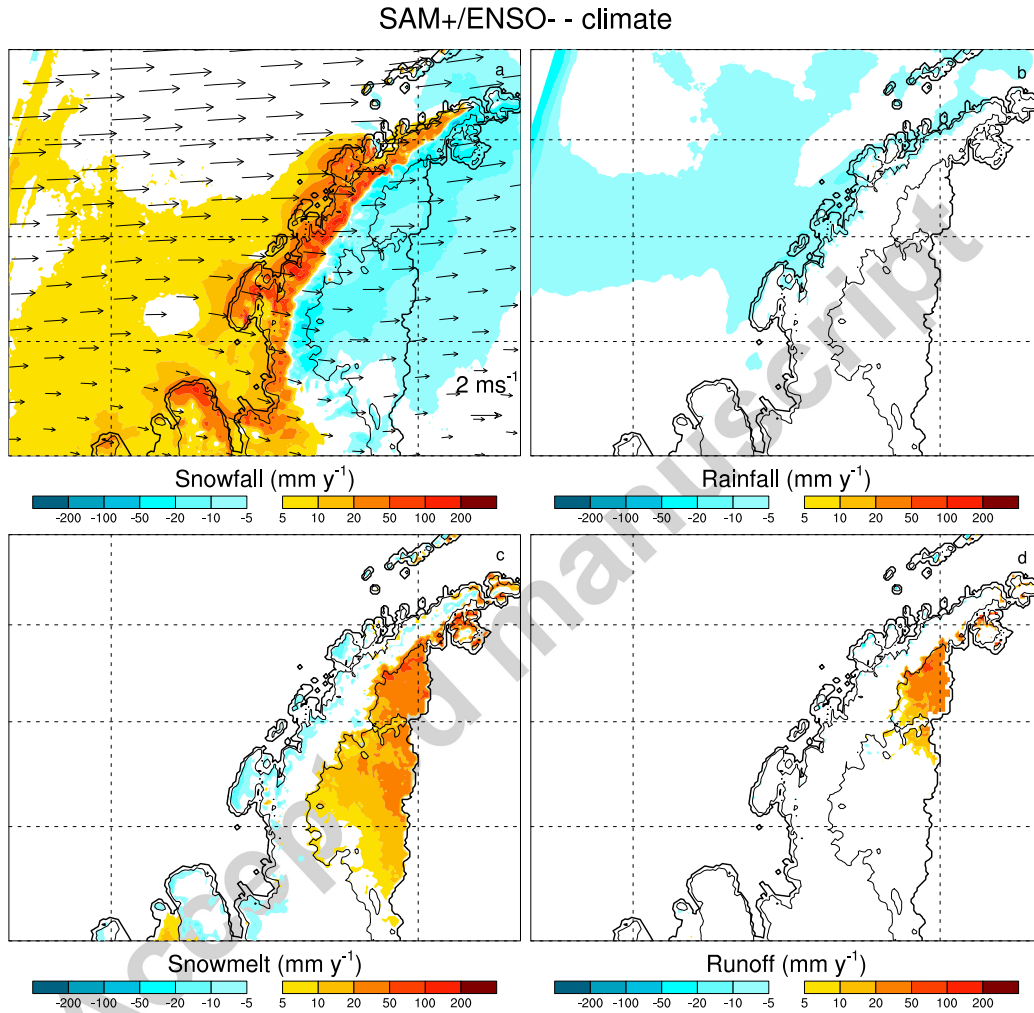


Figure 4: Difference of the SAM⁺/ENSO⁻ composite with the climatology (1979–2014) of the summer months (Dec., Jan., Feb.) freshwater components snowfall (a), rainfall (b), snowmelt (c) and meltwater runoff (d), in mm w.e. y⁻¹ for 1979–2014. In a) 500 hPa wind speed difference vectors are also shown. Details are found in Section 2.2.

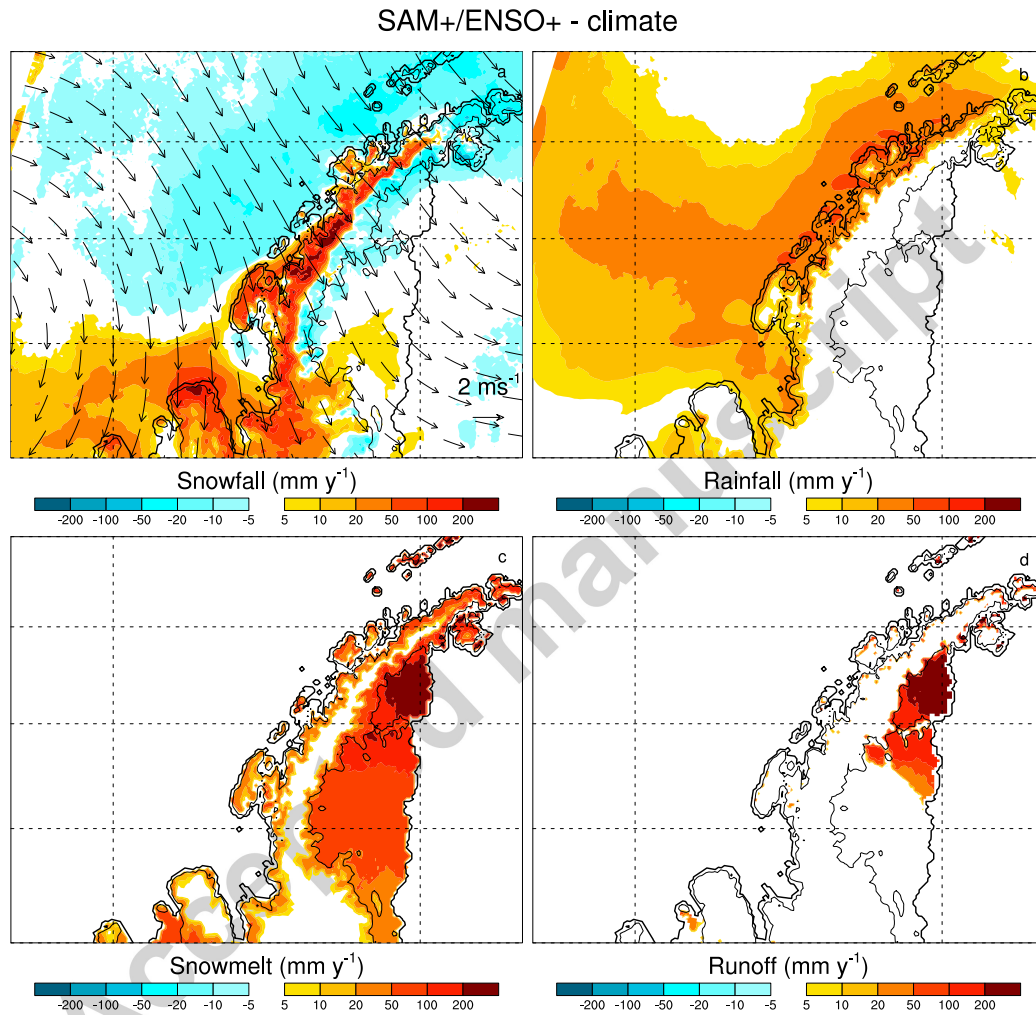


Figure 5: Difference of the SAM⁺/ENSO⁺ composite with the climatology (1979–2014) of the summer months (Dec., Jan., Feb.) freshwater components snowfall (a), rainfall (b), snowmelt (c) and meltwater runoff (d), in mm w.e. y⁻¹ for 1979–2014. In a) 500 hPa wind speed difference vectors are also shown. Details are found in Section 2.2.

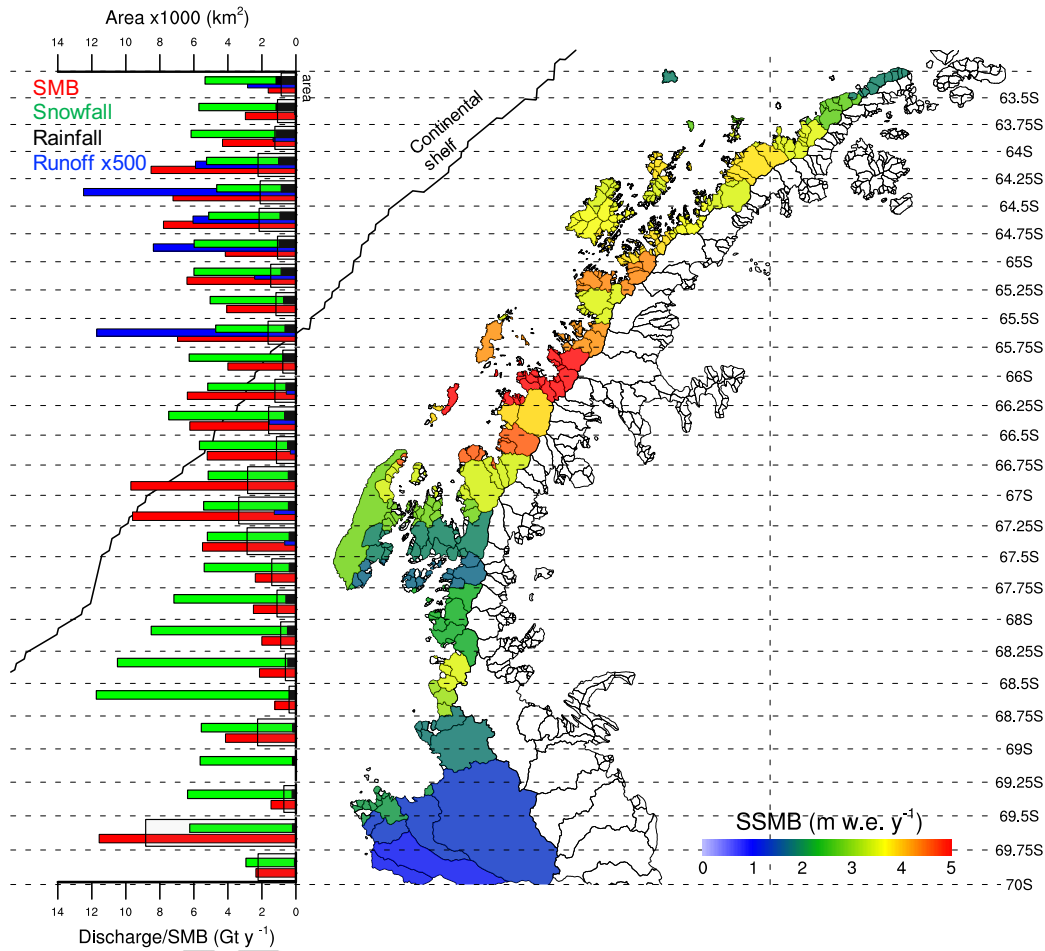


Figure 6: Specific (area averaged) surface mass balance (SSMB; m w.e. y⁻¹; colours), basin integrated SMB (Gt y⁻¹; red bars), meltwater runoff (500-Gt y⁻¹; blue bars), ocean integrated snowfall/rainfall (Gt y⁻¹; green/black bars) and area (1000· km²; black boxes) binned into 27 latitudinal intervals (0.25°). Only WAP basins larger than the area of one gridbox are used. Basin definitions are based on Cook et al. (2014). For each basin, the average latitude is calculated, which is used to determine to which bin the basin belongs. Ocean basins are based on all gridboxes up to the continental shelf (black line; see Fig. 1).